Effect of Geometry and Mass Distribution on Tumbling Characteristics of Flying Wings

C. M. Fremaux, D. M. Vairo, R. D. Whipple

Reprinted from

Journal of Aircraft

Volume 32, Number 2, Pages 404–410

A publication of the
American Institute of Aeronautics and Astronautics, Inc.
370 L'Enfant Promenade, SW
Washington, DC 20024-2518

JOURNAL OF AIRCRAFT
Vol. 32, No. 2, March–April 1995

Effect of Geometry and Mass Distribution on Tumbling Characteristics of Flying Wings

C. M. Fremaux* and D. M. Vairo†
Lockheed Engineering and Sciences Company, Inc., Hampton, Virginia 23666
and
R. D. Whipple‡
NASA Langley Research Center, Hampton, Virginia 23681

Results from an investigation to determine the low-speed tumbling characteristics of 12 generic flying-wing models are summarized. There is some concern that airplanes with flying-wing planforms could inadvertently enter an out-of-control tumbling motion under certain conditions. The objectives of this investigation were to 1) identify the geometric and mass-related parameters that cause flying wings to be capable of sustained tumbling and 2) analyze some of the driving mechanisms that cause steady tumbling. Free-tumble and free-to-pitch tests were conducted with dynamically scaled, generic flying-wing models. Results indicated that c.g. location, mass distribution, and geometric aspect ratio strongly affected the tumbling characteristics of the models tested and that positive static stability did not necessarily preclude tumbling. The magnitude of dynamic effects were found to be of the same order as static effects for the models undergoing autorotation-in-pitch.

Nomenclature

b	=	wing span, in.
C_l	=	lift coefficient
C_m	=	pitching moment coefficient
$C_{m_q} + C_{m_{\dot{\alpha}}}$	=	pitch damping derivative from forced-oscillation tests, $[\partial C_m/\partial(q\bar{c}/2V)] + [\partial C_m/\partial(\dot{\alpha}\bar{c}/2V)]$
$\bar{c}$	=	mean aerodynamic chord, in.
f	=	frequency of oscillation, cycles/s
H_m	=	stick-fixed static margin, $\%\ \bar{c}$
h_n	=	neutral point, $\%\ \bar{c}$
I_Y	=	model moment of inertia about the Y body axis, slug-ft^2
k	=	reduced frequency parameter for forced-oscillation tests, $\omega\bar{c}/2V$
m	=	mass of model, slugs
$\dot{q}$	=	angular acceleration about the Y body axis, rad/s^2
$\bar{q}$	=	freestream dynamic pressure, $\frac{1}{2}\rho V^2$, lb/ft^2
S	=	wing area, ft^2
V	=	wind-tunnel freestream velocity, ft/s
α	=	angle between fuselage centerline and the freestream (approximately equal to angle of attack for nontranslating model), deg
β	=	model sideslip angle, deg
Λ	=	wing leading-edge sweep angle, deg
ρ	=	air density, slugs/ft^3
ω	=	angular velocity, $2\pi f$, rad/s

Subscripts

avg	=	average
dyn	=	coefficient increment due to angular rates
LE	=	leading edge of wing
stat	=	static coefficient value
tot	=	total coefficient value representing the sum of static and dynamic components

Introduction

IN flight mechanics, the phenomenon of "tumbling" is defined as an autorotative pitching motion primarily about an axis parallel to a vehicle's lateral axis, plus translation in a vertical plane along an inclined flight path. Therefore, although tumbling is technically a six degree-of-freedom (6-DOF) motion (a slow precession of the vertical plane of motion can occur), it is essentially a 3-DOF motion. A potentially dangerous situation could develop if an aircraft were to enter a tumble. This article describes ongoing research on the tumbling characteristics of airplanes.

According to Dupleich,[1] some of the earliest work regarding the tumbling motion of wings was performed by Maxwell in 1853. Dupleich himself studied the tumbling of rectangular-planform, unswept wings in which the motion of the free-falling models was recorded on film for analysis.[1] Extensive wind-tunnel tests on tumbling were conducted in the 1940s by the National Advisory Committee for Aeronautics[2] (NACA). Fourteen dynamically scaled, free-flying models of actual or proposed aircraft were hand-launched into the vertically rising airstream of the Langley Aeronautical Laboratory 20-ft Free-Spinning Tunnel (now NASA Langley Research Center 20-ft Vertical Spin Tunnel) in order to document the tumbling characteristics of several different airplane configuration types, including conventional (wing-tail), canard (tail-wing), and several flying-wing designs. The potential detrimental effects on the pilot caused by the accelerations produced in a tumble were also assessed. In 1953, an analytical and experimental investigation was made by Smith[3] concerning the tumbling of the pilot-escape nose capsules of the Douglas D-558-1 and D-558-2 research airplanes, with consideration given to the different physical mechanisms that cause tumbling. In addition, an attempt has been made by researchers to use computational fluid dynamics (CFD) coupled with the flight dynamic equations to numerically simulate the tumbling motion of a rec-

Received Oct. 5, 1993; revision received July 13, 1994; accepted for publication July 22, 1994.

*Engineer, Advanced Aircraft and Flight Dynamics Section, 144 Research Drive. Member AIAA.
†Engineer, Advanced Aircraft and Flight Dynamics Section, 144 Research Drive.
‡Aerospace Technologist, Vehicle Dynamics Branch, M/S 343. Associate Fellow AIAA.

tangular flat plate.[1] Recent experimental and computational work at NASA Langley[2-6] has shown that a current airplane configuration with close-coupled canards (the X-29A) will tumble under certain conditions.

Of the aircraft configuration types examined in the foregoing studies, the general conclusion can be drawn that, other conditions being equal, flying wings are the most likely to tumble, whereas conventional configurations are least likely to tumble. Possible design trends of present and future advanced aircraft, including flying wings for both military and civil applications, warrant a renewed interest in tumbling research. To date there have been no published efforts to systematically identify the parameters that affect the tumbling characteristics of flying wings. In response, a research program was initiated to study various aspects of tumbling for generic flying-wing shapes. This article deals with the first phase of that research, with the overall objectives being to 1) identify the geometric and mass-dependent parameters that cause flying wings to be capable of sustained tumbling and 2) analyze some of the driving mechanisms that cause steady-state tumbling.

Experimental Methods

Dynamic Scaling

In order for the motion of an unconstrained model to be representative of its full-scale counterpart, the dynamic-scaling relationships[7] must be enforced (see Table 1). Applying these factors provides similitude between the model and full-scale article in terms of the fundamental dimensions of length, mass, and time for a given altitude and loading condition. Thus, the quantities listed in Table 1 can be directly converted to full-scale values by multiplying a given model quantity by the appropriate factor. It should be noted that in typical dynamically scaled tests, including those summarized in this article, Reynolds number similitude is usually not satisfied and the results must be interpreted with this in mind. The Reynolds number of the present tests was on the order of 1×10^6.

Models

Three sets of 12 flying-wing models were constructed (Fig. 1) for testing in both the 30- × 60-ft tunnel and spin tunnel at NASA Langley Research Center. The model numbers in this figure apply to all three sets and are used to distinguish between the different geometric shapes, and not the particular model used. The models represent a matrix of potential flying-wing planforms with a broad range of aspect ratios (AR = 1.6–7.4) and leading-edge sweep angles (Λ_{LE} = 28–60 deg). Wingspans for the free-to-pitch and free-tumble models are also shown in Fig. 1. The models were symmetrical about the X-Y and X-Z planes and had flat-plate airfoil sections with beveled leading and trailing edges for ease of construction (Fig. 2). In addition, it was assumed that the sharp leading and trailing edges would fix the separation points on the wings and thus help to minimize Reynolds number effects on the models. One set of models was used in the 30- × 60-ft tunnel to obtain static and dynamic data. These models were not dynamically scaled. Two sets of dynamically scaled models, both one-third scale versions of the 30- × 60-ft tunnel models, were used in the spin tunnel: the first set for free-tumble testing and the second set for testing on the free-to-pitch rig (the different wind-tunnel tests and the free-to-pitch rig are described in the next section). The free-to-pitch models had lower pitching moments of inertia than the free-tumble models to allow for the increase in total pitch inertia caused by the rotating parts of the free-to-pitch rig. Each model had a centerbody for housing a six-component strain-gauge balance in the case of the 30- × 60-ft tunnel models, or ballast in the case of the free-tumble and free-to-pitch models.

Table 1 Scale factors for dynamic models

	Scale factor
Linear dimension	N
Relative density, $m/\rho l^3$	1
Froude number, V^2/lg	1
Weight, mass	N^3/σ
Moment of inertia	N^5/σ
Linear velocity	$N^{1/2}$
Linear acceleration	1
Angular velocity	$N^{-1/2}$
Time	$N^{1/2}$
Reynolds number, Vl/ν	$N^{3/2}\sigma/\nu_0$

Note: Model values are obtained by multiplying airplane values by the following scale factors where N is the model-to-airplane scale ratio, σ is the ratio of air density to that at sea level (ρ/ρ_0), ν is the value of kinematic viscosity, l is a representative length, m is the vehicle mass, and g is the acceleration due to gravity.

For the free-tumble and free-to-pitch tests, stick-fixed static margin H_n was used as a basis for comparison of the results. The neutral points h_n used to calculate the static margins for both the tumble models and the flying-wing models of Ref. 2 were estimated using the method of Ref. 8. It is assumed in this method that the area of interest falls in the linear range of the C_m vs C_l curve. Therefore, the results are not strictly valid for tumble tests due to the large range of angle of attack encountered. However, the calculated neutral points were still considered to be useful as reference points for comparing the tumble behavior of the different models, and were used as such.

Test Techniques

Four types of low-speed wind-tunnel tests were conducted during this program: 1) static tests, 2) dynamic (forced-oscil-

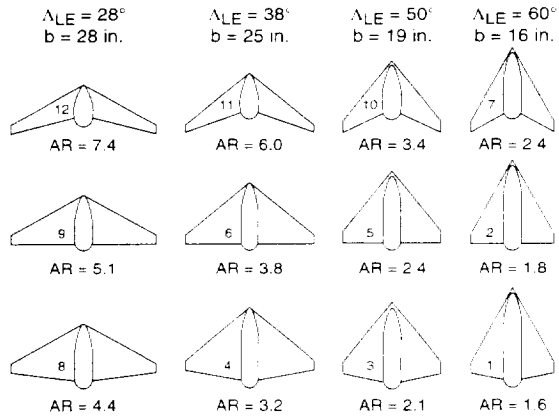

Fig. 1 Generic flying wing models used for tumbling research.

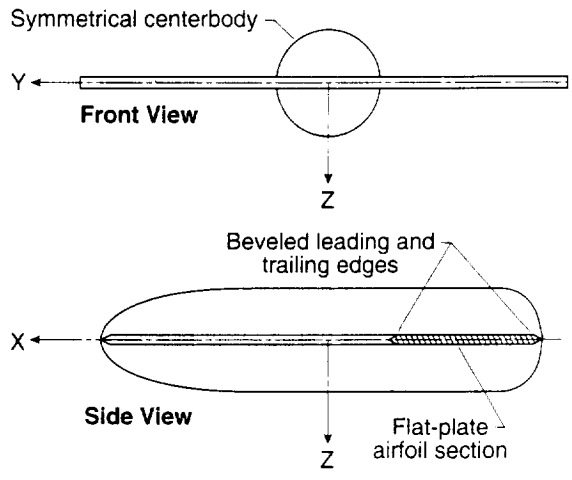

Fig. 2 Axis system and configuration features of typical tumble model.

lation) tests, 3) free-tumble tests, and 4) free-to-pitch tests. Each type of test is described briefly below in the context of the present research:

1) *Static tests* were conducted using the sting-supported 30- × 60-ft tunnel models. Each model was successively mounted on a six-component strain-gauge balance to obtain normal, axial, and side force coefficients, plus rolling moment, pitching moment, and yawing moment coefficients at angles of attack α ranging from 0 to 180 deg and 0 to −180 deg in 2-deg increments at sideslip angles β of 0, −5, and +5 deg.

2) *Forced-oscillation tests* were also conducted using the 30- × 60-ft tunnel models to obtain the "lumped" pitch damping derivative due to oscillation about the pitch axis ($C_{m_q} + C_{m_{\dot{\alpha}}}$). A thorough description of this technique appears in Ref. 9, but a brief synopsis of a typical test is given here.

For a typical test, a model was set at a nominal angle of attack on the forced-oscillation rig (Fig. 3). After the tunnel was brought up to the desired velocity, an electric drive motor was started, causing the rig to begin oscillating about that angle of attack at a reduced frequency parameter k of 0.5. The amplitude of the oscillations was fixed at ±5 deg by the gearing of the drive mechanism. Data were then obtained via a data-acquisition computer. The procedure was then repeated for each desired angle of attack.

3) *Free tumble (6-DOF) tests* were conducted in the spin tunnel with one set of the small models dynamically scaled to represent realistic full-scale aircraft. These models were hand-launched into the vertically rising airstream of the spin tunnel, and the resulting motion as they traversed the test section was recorded on high-resolution video tape for later analysis. During a typical test, a model either underwent several tumble cycles before striking the safety net, or the pitching motion damped out and the model dove into the bottom of safety net. In a third possible scenario, the model would transition from primarily rotation-in-pitch to rotation about all three axes a few cycles after launch, in which case the test would be labeled as "no tumble." Although transient in nature, free-tumble tests provided a useful "yes-no" answer to the question "will it tumble?." Data were obtained as a function of the degree of static longitudinal stability (i.e., c.g. location), mass distribution (moments of inertia about all three axes), and whether or not an initial nonzero pitch rate was imparted to the models at launch. Note that the quantity "α" in this report and the actual angle of attack do not coincide for free tumbling due to the translation inherent in this type of motion.

4) *Free-to-pitch (1-DOF) tests* were conducted with a second set of small models that were dynamically scaled in pitch and mounted on a free-to-pitch rig that could be easily installed in the spin tunnel. The rig was instrumented with an optical encoder and computerized data acquisition system that allowed a time history of the model angular attitude to be recorded in test runs of any desired length. The mounting fixtures were adjustable so that the axis of rotation coincided with the c.g. location. Friction in the rotating parts of the rig was minimized by using ball bearings that were estimated to result in a total resisting pitching moment coefficient of less than 0.001 under the most extreme test conditions encountered. By definition, shaft rotation is not tumbling since three translational and two rotational DOF have been precluded. Following Smith,[3] this motion has been labeled "autorotation in pitch" in this article. However, it has been suggested[3] that autorotation in pitch is a reasonable representation of tumbling that allows quantitative data to be obtained. In free-to-pitch tests, α and the true angle of attack are forced to be the same (assuming that the freestream is truly vertical), due to the absence of translation.

In all of the free-to-pitch tests, only steady-state data were obtained due to limitations of the rig design. For the tests, the models were given an impulsive "push" to start rotation, although neither the pitch rate nor the pitch angle at which the model began autorotating were known. If the model continued to rotate from "launch," then data were obtained over several cycles. Future modifications to the rig are planned so that models can be prerotated at a known pitch rate and then released at a known pitch angle. In this way, information on the transient motion before a model reaches steady state will be available. This information would allow analysis of the onset of autorotation and, presumably, the prediction of the onset of tumbling.

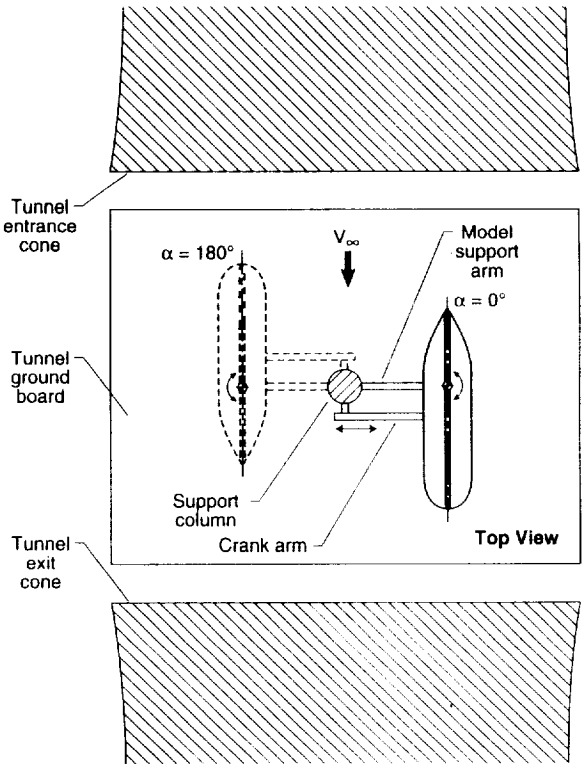

Fig. 3 Tumble model mounted on forced oscillation rig in 30- × 60-ft tunnel.

Tumble Simulations

Although not addressed in this article, simulations were developed with the initial goal of predicting steady tumbling or autorotation in pitch of flying wings. The reader is directed to Ref. 10 for a discussion of the initial simulation development for tumbling undertaken during this research.

Results and Discussion

Results of the free-tumble and free-to-pitch studies will be discussed in this section. Data from the static and forced-oscillation test were used in a supporting role and will not be discussed extensively.

Free-Tumble Tests

For free-tumble tests, 12 small models were hand-launched into the vertical airstream of the spin tunnel. As a starting point, the mass and dimensional characteristics of the XB-35 Flying Wing bomber[7] at its nominal c.g. position (27.5% $\bar{c}$) were used for the initial scaling of model 12 (Λ_{LE} = 28 deg, AR = 7.4) with a scale factor N of 31 (see Table 1) at a simulated test altitude of 25,000 ft. Changes in c.g. position from that of the XB-35 were accompanied by changes in the inertial characteristics. The other models were also ballasted to cover a range of c.g. locations and inertial characteristics, but without regard to the characteristics of any particular airplane configuration.

For each of the loading conditions tested, two types of launch technique were used: 1) the "forced launch" technique in which the models were given an initial pitch rate (positive,

or nose-up as the model translated across the test section); and 2) the "tail slide" technique in which the launcher released the model tail-first into the vertical airstream with no initial pitch rate. Certain model configurations tumbled only when forced launches were used, while others tumbled using either technique. To ensure the repeatability of the data, each combination of loading and launch method was tested several times.

Some free-tumble test results appear in Fig. 4. In this figure, the inertia yawing moment parameter (IYMP) of each condition tested is plotted as a function of the stick-fixed static margin H_m obtained by varying the c.g. locations for each of the 12 models. It is well known[11] that the free rotation of a rigid body is stable only about the axes with the largest and smallest moments of inertia, and unstable about the axis of intermediate moment of inertia. This is necessarily true only in the absence of external influences acting on the body. Clearly, potentially large aerodynamic moments are present during tumbling (e.g., rolling moment), so that it was not evident from the outset that the inertial characteristics of the models would dominate their motion. However, Fig. 4 shows that a sustained tumble was indeed possible only for models tending towards a wing-heavy loading (i.e., IYMP > 0 or $I_x > I_y$). With wing-heavy loadings, model motions were essentially 3-DOF in nature. In all cases, I_y was either the smallest or intermediate moment of inertia. Testing whether or not the models would tumble with I_y as the largest moment of inertia was not practical due to the ballasting constraints of the flying-wing configurations (i.e., I_z will always tend to be the largest of the three). For tests where IYMP < 0, the motion of the models quickly transitioned from rotation in pitch to rotation about all three axes, and the run was labeled no tumble as described previously. Two data points from Ref. 2 were plotted for comparison with good correlation to the present results. These tests indicated that tumbles were possible for certain models even with a positive (statically stable) H_m.

Figure 5 is a plot of H_m as a function of model quarter-chord sweep angle $\Lambda_{1/4}$. For a given $\Lambda_{1/4}$, the most forward c.g. location tested that produced a tumble and the next most forward c.g. location tested that did not produce a tumble are plotted. Only data for wing-heavy test conditions (IYMP > 0) were considered, ensuring that model motions were 3-DOF. Therefore, any no tumbles were due to the pitch rate damping out, and not due to the models rotating about their roll and yaw axes. In this way, the effects of changing wing sweep on tumbling were isolated from any inertial effects. Due to practical limitations in ballasting, the most forward c.g. limits that produced tumbles were not found for models 1 (AR = 1.6), 2 (AR = 1.8), and 7 (AR = 2.4), although all three models did tumble for the condition IYMP > 0.

No clear pattern of tumble characteristics emerges when the data are plotted in this manner, although three distinct groups of points are evident. These groups represent the first three columns of models in Fig. 1 (i.e., Λ_{LE} = 28 deg, Λ_{LE} = 38 deg, Λ_{LE} = 50 deg). However, it is impossible to isolate the effects of changing wing sweep from that of changing aspect ratio because aspect ratio was different for each model, as noted in the figure. Examination of Fig. 5 indicates that the H_m for tumble or no tumble increased as aspect ratio increased. Evidently, a model's aspect ratio had a strong influence on its tendency to tumble or not tumble.

Figure 6 illustrates that a "tumble boundary" is formed when the data are replotted with H_m as a function of model geometric aspect ratio. The size of the transition zone (the dashed region) was determined by the spacing of the tests in terms of the c.g. location required to produce a tumble or no tumble. This figure shows that for aspect ratios of 3.2 and above, tumbles were possible with stable (positive) static margins. In fact, tumbles were obtained with $H_m \approx +10\%$ for the highest aspect ratio tested (model 12, AR = 7.4). Conversely, model 3 (AR = 2.1) required a negative static margin ($H_m \approx -5\%$) for tumbling to occur.

Four data points from Ref. 2 are plotted in Fig. 6 for comparison. These data correspond to cases with neutral pitch controls on the models in Ref. 2, which would be the most similar to the models of the present test with fixed trailing edges. The tumble points for both the XB-35 and XP-79 fall within the tumble region of the present test. However, the no-tumble point of the XB-35 also falls within the tumble region by a static-margin difference of about 1% $\bar{c}$. Two possible explanations for this discrepancy are evident. First, both the XB-35 and XP-79 airplanes employed very thick airfoil sections (18%). In contrast, the tumble models for the present tests had flat-plate airfoil sections with sharp leading and trailing edges as discussed previously. Inasmuch as both tests were performed in the same facility at approximately the same (very

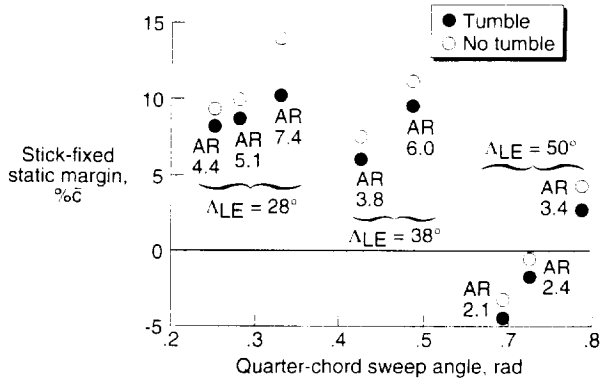

Fig. 5 Static margin for tumble as a funtion of wing sweep for models with wing-heavy loadings.

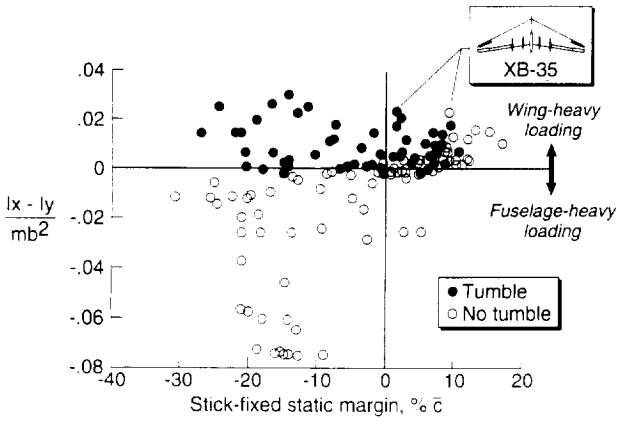

Fig. 4 Free-tumble results for 12 flying wing models at all mass loadings examined.

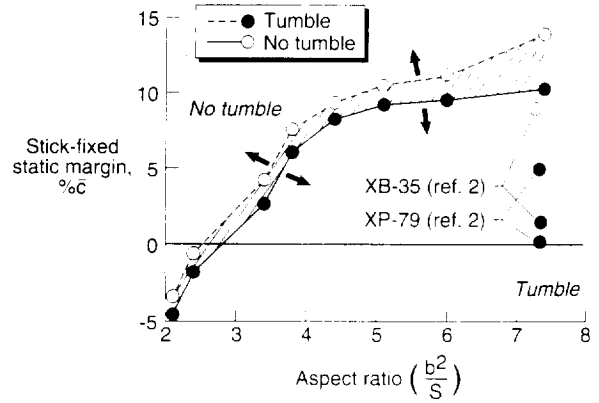

Fig. 6 Static margin for tumble as a function of aspect ratio for models with wing-heavy loadings.

low) Reynolds number, it is likely that the discrepancy noted in Fig. 6 is primarily due to Reynolds number effects on the rounded, relatively large-radius leading edges of the XB-35 and XP-79 models. In addition, both of the earlier models had protuberances representing engine nacelles, canopies, vertical tails, etc., whereas the free-tumble models had a single, large center section to house ballast. These differences would make a direct comparison of the tumble/no-tumble points based only on c.g. position and aspect ratio difficult due to potentially significant differences in pitching moment characteristics.

Another point of interest in Fig. 6 is that the static margin values defining the tumble/no-tumble boundary appear to be approaching a maximum as the aspect ratio increases. This probably indicates that a maximum positive static margin beyond which tumbling will not occur, regardless of how high the aspect ratio becomes, was being approached. However, it is unlikely that this limiting value of H_n was reached during these tests. It is re-emphasized that the effects of both aspect ratio and wing sweep on tumbling are included in Fig. 6 (as well as in Fig. 5), and that two different sets of models, one with constant aspect ratio but varying sweep and the other with constant sweep but varying aspect ratio, would be needed to differentiate between the effects of these two parameters on tumbling.

Free-to-Pitch Tests

Six of the twelve model geometries used in the free-tumble tests [models 4, 6, 11, 8, 9, and 12 (Fig. 1)] were also tested on the free-to-pitch rig. These models were chosen because they had the highest aspect ratios [with the exception of model 4 (AR = 3.2) that was tested, and model 10 (AR = 3.4) that was not]. Based on the free-tumble results, these higher aspect ratio models tended to have the greatest propensity for tumbling, and presumably, autorotation in pitch.

In Fig. 7, results from the free-to-pitch tests are superimposed on the free-tumble data of Fig. 6. Note that the trend of static margin required to prevent tumbling becoming generally more positive as AR increased is still evident. However, the transition zones do not overlap above AR = 3.5. Beyond this point, the free-to-pitch models would not tumble with a c.g. as far forward as their free-tumble counterparts. In addition, the gap between the two sets of data widens as aspect ratio increases. It is suggested that the following three effects could produce this divergence in the data:

1) *Differences in total pitching moment between rig-mounted and free-tumbling models.* According to Smith,[3] restraining a body from 6-DOF (free-tumble) to 1-DOF (shaft) motion can remove potential driving mechanisms of tumbling. For example, the c.g. of a free-tumbling model follows a wavy path (even if the motion is essentially 3-DOF) due to large variations in lift and drag over a cycle. This effect could cause incremental driving (or retarding) moments to develop during free tumbling due to variations in dynamic pressure that would not be present during rotation about a shaft. If these incremental moments were phased such that the total driving moment was increased as compared to that produced by 1-DOF shaft rotation, then free-tumbling would be possible even if autorotation in pitch on a shaft were not. In addition, other effects due to translation, such as changes in local angle of attack of the model, may add to the discrepancy between free-tumble results and free-to-pitch results.

2) *Free-to-pitch rig bearing friction.* There is a small but relatively constant resisting moment produced by the ball bearings of the free-to-pitch rig. Thus, "borderline" cases where the net propelling moments were smaller than the resisting bearing moments would not undergo autorotation on the rig. Bearing friction estimates for the rig were discussed in a previous section.

3) *Aerodynamic interference between the model and free-to-pitch rig.* Changes in the flowfield around a model mounted on the rig could potentially change the autorotation characteristics of the model as compared to the same model undergoing free tumbling. The extent of any aerodynamic interference between the rig and a model autorotating in pitch has not been assessed, but it is likely that some modification of the flowfield around the model due to interference does exist.

While not duplicating the tumble/no-tumble boundary from the free-tumble results, the free-to-pitch data are useful nonetheless. An estimate of the total pitching moment coefficient $C_{m_{tot}}$ may be extracted by making use of the 1-DOF equation of motion for a body rotating in pitch:

$$C_{m_{tot}} = I_y \ddot{\alpha}/\bar{q}S\bar{c} \tag{1}$$

All of the quantities on the right side of Eq. (1) are known constants for a given set of test conditions, with the exception of the pitch acceleration $\dot{q} = \ddot{\alpha}$. Using a time history of a model's pitch attitude over a given cycle obtained with the free-to-pitch rig's optical encoder (see Fig. 8 for a description of model attitude over a cycle), the data were fitted with a high-order polynomial and differentiated to yield the pitch rate ($q = \dot{\alpha}$), and then again to obtain the pitch acceleration ($\dot{q} = \ddot{\alpha}$) in Fig. 9. For illustration, this procedure was applied to data from model 9 undergoing steady autorotation in pitch. The calculated $C_{m_{tot}}$ was then plotted over a full cycle as a function of model angle of attack α to obtain Fig. 10. Note that this figure represents the total of all external effects on the model (both static and dynamic) as well as inertial effects. Beginning at the center of Fig. 10 ($\alpha = 0$ deg) and following the arrows, it is seen that the model motion (pitching "nose-down" in all cases) was being resisted in the first part of the cycle from $\alpha = 0$ deg to $\alpha = 160$ deg. The model was already undergoing steady-state autorotation before entering this cycle, and its angular momentum carried it through a region where the motion was resisted. It then became propelling for most of the remainder of the cycle until the motion was again resisted from $\alpha = 25$ deg through the end of the cycle at $\alpha = 0$ deg. No attempt was made to remove the moment contribution due to bearing friction from $C_{m_{tot}}$, because its effect on the trends in Fig. 10 were assumed to be only a small

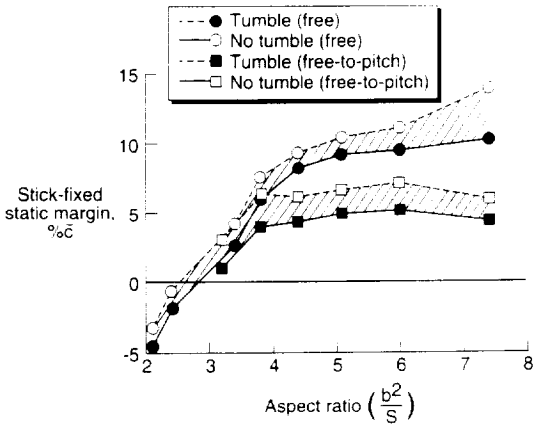

Fig. 7 Static margin for tumble with wing-heavy loadings or autorotation in pitch as a function of aspect ratio.

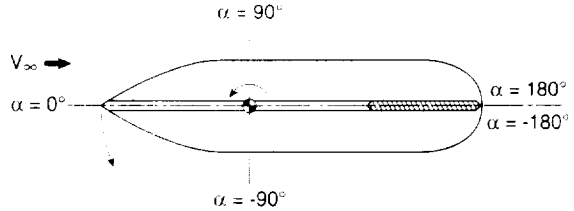

Fig. 8 Model pitching nose down on the free-to-pitch rig.

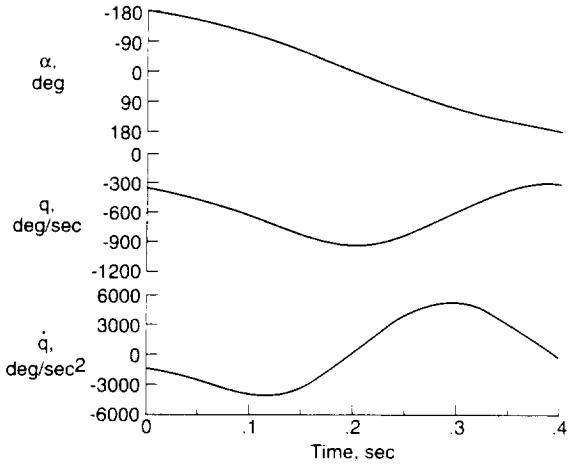

Fig. 9 Attitude, pitch rate, and pitch acceleration of model 9 over one cycle on the free-to-pitch rig.

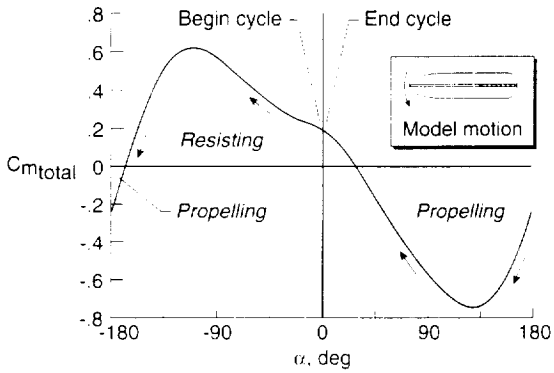

Fig. 10 Total pitching moment coefficient of model 9 over one cycle on the free-to-pitch rig.

upward displacement of the data, and not a change in the shape of the curve.

Although the aerodynamics of tumbling are complex due to the presence of high rotation rates, large angular displacements, and separated flow during large parts of a tumble cycle, it is useful to assume that a simple model of total pitching moment is applicable so that an initial analysis can be carried out. The total pitching moment coefficient can be written as the sum of static and dynamic terms, and Eq. (1) becomes

$$C_{m_{\text{tot}}} = C_{m_{\text{stat}}} + C_{m_{\text{dyn}}} \tag{2}$$

$C_{m_{\text{dyn}}}$ was calculated using static pitching moment data from the 30- × 60-ft tunnel tests and the total pitching moment data represented by Fig. 10. Figure 11 shows the relative contributions of the static and dynamic pitching moments for the cycle under consideration. Dynamic effects were of the same order of magnitude as static effects for most of the cycle during the steady, autorotative pitching motion. This is in contrast to the small-amplitude, lower-rate motions typical of a maneuvering airplane where the total pitching moment would still tend to be dominated by static effects throughout large portions of the angle-of-attack range.

Using the above assumptions, the pitch damping derivative (analogous to the $C_{m_q} + C_{m_{\dot\alpha}}$ from forced-oscillation tests and termed "pitch damping" here for brevity) of a model undergoing autorotation pitch can be estimated. For 1-DOF, the dynamic pitching moment coefficient can be rewritten as the product of a pitch damping term and a nondimensional pitch rate, or

$$\begin{aligned} C_{m_{\text{dyn}}} &= (\text{pitch damping})(q\bar{c}/2V) \\ \therefore \text{pitch damping} &= (C_{m_{\text{dyn}}})(2V/q\bar{c}) \end{aligned} \tag{3}$$

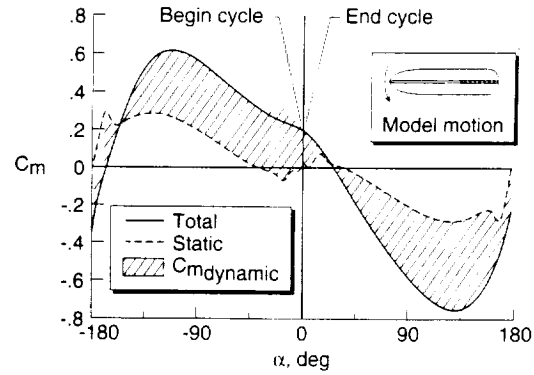

Fig. 11 Total, static, and dynamic pitching moment coefficients of model 9 over one cycle on the free-to-pitch rig.

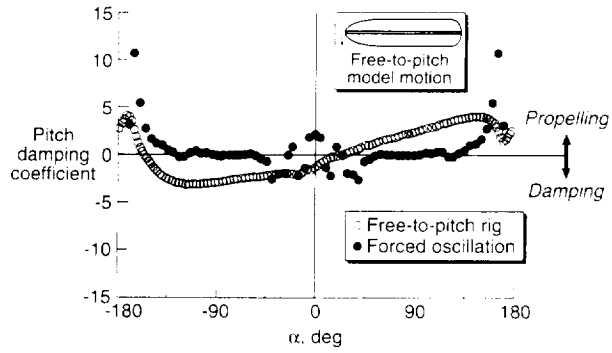

Fig. 12 Pitch damping derivative of model 9 measured on the forced oscillation rig and estimated using free-to-pitch data.

The pitch damping term was calculated using $C_{m_{\text{dyn}}}$ obtained previously, and q, V, and $\bar{c}$ from the free-to-pitch tests of model 9. A sample result is shown in Fig. 12, where pitch damping is plotted as a function of α. The pitch damping derivative $C_{m_q} + C_{m_{\dot\alpha}}$ from the forced-oscillation tests in the 30- × 60-ft tunnel are also plotted for comparison. Recall that the model 9 was rotating in a nose-down direction on the free-to-pitch rig. Differences between the free-to-pitch data and the forced-oscillation data are evident. For example, the forced-oscillation method predicted neutral dynamic stability (pitch damping = 0) in the regions 45 deg > α > 135 deg and −45 deg > α > −135 deg. As expected, the results were quite different for the model undergoing a continuous, high-rate pitching motion.

In contrast to the forced-oscillation results, the estimated pitch damping data from the free-to-pitch tests indicated significant propelling and damping regions throughout the cycle. Again examining Fig. 12, the free-to-pitch cycle began at α = 0 deg and continued in the negative direction. The motion was dynamically damped for most of the half-cycle up to α = −160 deg. Beyond α = −160 deg the motion was propelling until α = 20 deg, and damped for the remainder of the cycle (back to α = 0 deg). Clearly, large regions of neutral dynamic pitch stability did not exist for this model undergoing autorotation in pitch.

Summary and Conclusions

Tumbling is a potential concern for tailless or "flying-wing" aircraft. As such, tumbling research is important not only for present and future military aircraft, but also to potential civil applications such as the "spanloader" concept. In this article, an effort has been made to identify some of the parameters that cause a configuration to be capable of a sustained tumbling motion through the use of dynamically scaled generic models that represent a broad matrix of flying-wing planform shapes. "Tumble boundaries" for the models tested are pre-

sented as a function of stick-fixed static margin and model aspect ratio. Some models were found to tumble even though they were statically stable. Effects due to changing mass distribution and wing sweep are presented. Some of the characteristics of a model undergoing steady autorotation in pitch are explored. Further work is needed to be able to predict the onset of tumbling, possibly by obtaining and modeling transient data from the free-to-pitch rig. Dynamically scaled drop-model tests could also be used to determine the susceptibility of flying wings to depart into a tumble from controlled flight. The ability of aerodynamic controls to both drive and halt a developed tumble should be explored. Potential Reynolds number effects on tumbling characteristics should be further addressed as should the effects of aerodynamic interference on data obtained on rotating rigs.

Acknowledgment

The authors would like to thank M. A. Croom (Aerospace Technologist, Vehicle Dynamics Branch) for providing the static and forced-oscillation data obtained in the 30- × 60-ft tunnel.

References

[1]Dupleich, P., "Rotation in Free Fall of Rectangular Wings of Elongated Shape," NACA TM 1201, April 1949.

[2]Stone, R. W., Jr., and Bryant, R. L., "Summary of Results of Tumbling Investigations Made in the Langley 20-Foot Free-Spinning Tunnel on 14 Dynamic Models," NACA RM L8J28, Dec. 1948.

[3]Smith, A. M. O., "On the Motion of a Tumbling Body," *Journal of the Aeronautical Sciences*, Vol. 20, No. 2, 1953, pp. 73–84.

[4]Gallaway, C. R., and Hankey, W. L., "Free-Falling Autorotating Plate—A Coupled Fluid and Flight Mechanics Problem," *Journal of Aircraft*, Vol. 22, No. 11, 1985, pp. 983–987.

[5]Whipple, R. D., Croom, M. A., and Fears, S. P., "Preliminary Results of Experimental and Analytical Investigations of the Tumbling Phenomenon for an Advanced Configuration," AIAA Paper 84-2108, Aug. 1984.

[6]Fears, S. P., "Investigation of the Tumbling Phenomenon Using Computer Simulation," M.S. Thesis, George Washington Univ., Washington, DC, Sept. 1985.

[7]Chambers, J. R., "Use of Dynamically Scaled Models for Studies of the High-Angle-of-Attack Behavior of Airplanes," International Symposium on Scale Modeling, Tokyo, Japan, July 1988.

[8]Etkin, B., *Dynamics of Flight, Stability and Control*, 2nd ed., Wiley, New York, 1982, pp. 353–359.

[9]Chambers, J. R., and Grafton, S. B., "Static and Dynamic Longitudinal Stability Derivatives of a Powered 1/9-Scale Model of a Tilt-Wing V/STOL Transport," NASA TN D-3591, Sept. 1966.

[10]Fremaux, C. M., Vairo, D. M., and Whipple, R. D., "Effect of Geometry, Static Stability, and Mass Distribution on the Tumbling Characteristics of Generic Flying Wing Models," *AIAA Atmospheric Flight Mechanics Conference*, AIAA, Washington, DC, 1993, pp. 1–11.

[11]Torby, B., *Advanced Dynamics for Engineers*, 1st ed., Holt, Rinehart and Winston, New York, 1984, pp. 354, 355.